Mechanical Characterization of Released Thin Films by Contact Loading

Rongjing Zhang
Division of Engineering and Applied Science,
California Institute of Technology,
Pasadena, CA 91125

Doron Shilo
Faculty of Mechanical Engineering,
Technion—Israel Institute of Technology,
Haifa 32000, Israel

Guruswami Ravichandran

Kaushik Bhattacharya

Division of Engineering and Applied Science,
California Institute of Technology,
Pasadena, CA 91125

The design of reliable micro electro-mechanical systems (MEMS) requires understanding of material properties of devices, especially for free-standing thin structures such as membranes, bridges, and cantilevers. The desired characterization system for obtaining mechanical properties of active materials often requires load control. However, there is no such device among the currently available tools for mechanical characterization of thin films. In this paper, a new technique, which is load-controlled and especially suitable for testing highly fragile free-standing structures, is presented. The instrument developed for this purpose has the capability of measuring both the static and dynamic mechanical response and can be used for electro/magneto/thermo mechanical characterization of actuators or active materials. The capabilities of the technique are demonstrated by studying the behavior of 75 nm *thick amorphous silicon nitride* (Si_3N_4) *membranes. Loading up to very large deflections shows excellent repeatability and complete elastic behavior without significant cracking or mechanical damage. These results indicate the stability of the developed instrument and its ability to avoid local or temporal stress concentration during the entire experimental process. Finite element simulations are used to extract the material properties such as Young's modulus and residual stress of the membranes. These values for* Si_3N_4 *are in close agreement with values obtained using a different technique, as well as those found in the literature. Potential applications of this technique in studying functional thin film materials, such as shape memory alloys, are also discussed.* [DOI: 10.1115/1.2166652]

1 Introduction

An important aspect in advancing the application of Micro/Nano Electro-Mechanical Systems (MEMS/NEMS) is to increase the reliability of the component devices. This largely depends on the knowledge and understanding of the mechanical behavior of the component materials [1–3]. However, the mechanical characterization of active materials and associated MEMS devices has lagged behind the corresponding theory and design software [1]. Standard methods for characterization have yet to be established. For these purposes, mechanical characterization instruments, which allow testing structures with small dimensions such as thin free standing films, membranes, and cantilevers, are required. The interest in reducing the dimensions of these structures to increase the volume density warrants load and displacement sensitivity in the sub-mN and sub-μm scales. These requirements are not met by the traditional mechanical characterization tools, such as the large scale materials testing machines. On the other hand, nano-indentation systems [4] are suitable for local characterization of thin films on substrates, but not for free-standing micro device characterization. Therefore, there is a great interest in developing new techniques that allow for testing in the gap between the capabilities of the above mentioned well established instruments, between macro and nano scales.

Recently, many efforts in new testing methods were made by different research groups to explore the mechanical properties on free standing thin films [5–17]. These methods typically impose a fixed displacement by means of a nano-positioning motor [10–16] or an on-chip actuator [17] and measure the load. Displacement-control experiments are suitable for large specimens and/or for ductile materials, which exhibit relatively high fracture toughness. However, the fragile nature and nonlinear behavior of many component materials in MEMS structures raise the possibility of having a sudden unexpected load, which may cause failure under displacement control. For example, when starting the experiment and approaching the tip to the sample, there is always a sudden change in load which requires a feedback loop to prevent damage to the sample. Moreover, many thin MEMS structures present strong nonlinearity in load displacement relations. When these relations are unknown, there exists the possibility for high loading rate when apply a pre-determined displacement rate to these thin structures. Therefore, it is desirable to test fragile MEMS structures in a load-control instrument, i.e., an instrument that imposes a force and measures the displacement. Displacement-control instruments can be adapted for load control by means of a feedback loop. But, there are severe limitations on the response time and this is effective only for quasi-static tests instead of dynamic testing. Hence, there is a necessity to develop new techniques, which operate under load control for measuring mechanical properties of fragile MEMS devices.

Many of the MEMS structures can be studied only by dynamic load controlled experiments. These include micro-actuators, which are evaluated by the load they can overcome, and active materials such as shape memory alloys, electrostrictive, and magnetostrictive materials, in which the load (i.e., the stress and not the strain) determines the driving force for microstructural changes such as domain switching [18,19]. These advanced functional devices require a combination of a controlled and constant mechanical load and a dynamic electric/magnetic/thermal loading. Such experiments are currently beyond the scope of existing techniques.

This paper presents a new technique for measuring the mechanical response of thin free-standing MEMS structures under load control. The apparatus developed consists of inexpensive off-

Contributed by the Applied Mechanics Division of ASME for publication in the JOURNAL OF APPLIED MECHANICS. Manuscript received July 5, 2005; final manuscript received November 16, 2005. Review conducted by K. Ravi-Chandar. Discussion on the paper should be addressed to the Editor, Prof. Robert M. McMeeking, Journal of Applied Mechanics, Department of Mechanical and Environmental Engineering, University of California—Santa Barbara, Santa Barbara, CA 93106-5070, and will be accepted until four months after final publication in the paper itself in the ASME JOURNAL OF APPLIED MECHANICS.

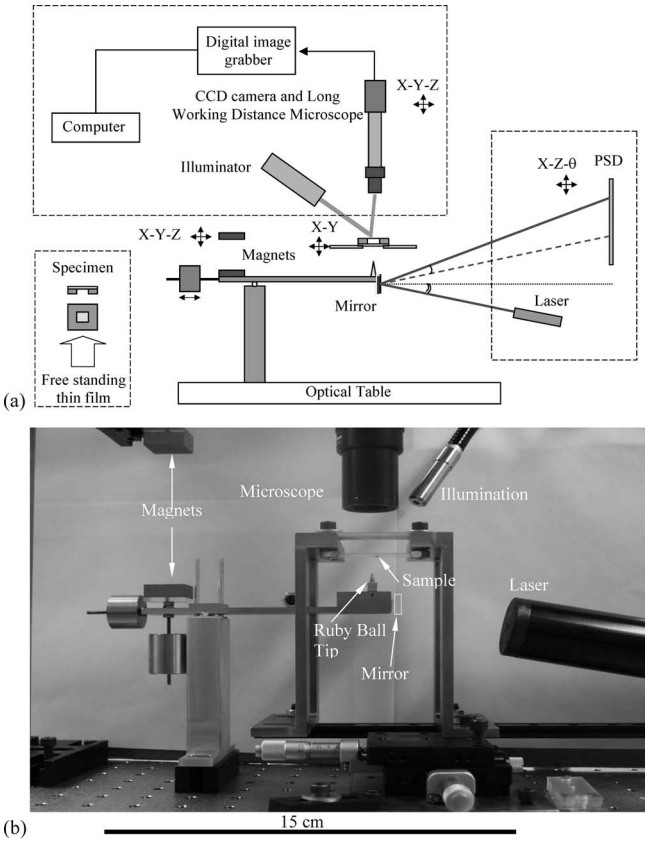

Fig. 1 (*a*) Schematic illustration of the experimental setup; (*b*) Photograph of the experimental apparatus

the-shelf products and can also be used for dynamic electro/magneto/thermo mechanical characterization experiments. The capabilities of the technique are demonstrated by testing the behavior of amorphous Si_3N_4 membrane structures, and the results demonstrate an ability to avoid local or transient stress concentration during the entire experiment.

2 Experimental Setup

The requirement of the loading and displacement range, as well as the fragility of the sample increase the difficulties in designing mechanical characterization methods for MEMS devices. The traditional methods for displacement measurement, such as the strain gauge and LVDT (linear variable displacement transducer), require partial or entire sensor in contact with the surface whose displacement needs to be measured. These methods are limited in use on the fragile sub-micron thick free-standing thin films and membranes. To overcome these difficulties, a noncontacting method using a laser beam and a position sensitive detector (PSD) are used.

Designing an appropriate loading method for testing thin films is also challenging. In principle, load control can be obtained if the spring constant of the apparatus, i.e., the mechanical structure that transmits the load from the actuator to the specimen, is significantly smaller than that of the specimen. In this situation, the applied force, F, is directly determined by the displacement imposed by the actuator, S, via $F \cong K_0 S$ where K_0 is the effective spring constant of the apparatus. However, this condition requires a very small value of K_0, which results in a low resonant frequency of the apparatus and limits the application of dynamic experiments. This problem is overcome by applying the load via a magnetostatic interaction in which the response time is much faster.

A schematic of the experimental setup is shown in Fig. 1(*a*) and a photograph of the principal apparatus is shown in Fig. 1(*b*). The load is applied by a tip, which is attached to one end of a substantially rigid beam. The force applied to the sample is proportional to the magnetostatic force being applied to the other end of the rigid beam. The late force is controlled by changing the distance between a pair of permanent magnets; one (lower) is attached to the beam and the other (upper) is attached to an external post and is able to move vertically. The upper magnet is aligned in the horizontal plane, using a *X-Y* micro-stage, such that it is situated exactly above the lower magnet, and hence no lateral forces are applied on the rigid beam.

A wide variety of methods have been suggested in the literature for measuring specimen displacements (or strains) in micromechanical testing apparatuses. These include imaging techniques [10–13], interference patterns [14,15], diffraction spots [16], and capacitance measurements [17]. These methods are limited by low sampling rates, or not having high enough resolution for large deformation, or the special complicated manufacture and sensing process of the censor. Some of these methods need special treatment (e.g., reflective coating) of the samples, which can alter the sample structure. In order to enable dynamic experiments, the loading tip displacement, which is the same as the displacement of the sample at the contact point, is measured by monitoring the deflection of a single laser beam, which is reflected from a mirror attached to the end of the rigid beam. The reflected laser beam is sensed by a Position Sensitive Detector (PSD) (Hamamatsu Co., S3979), which is attached to an external post, and the resulting voltage signal is recorded using an oscilloscope (LDS Nicolet Technologies, Model 40) (see Fig. 1). The PSD circuit allows sampling rates of up to 100 kHz and has a typical precision of about 1 μm. Due to a geometric amplification (the distance between the mirror and the PSD is typically 10 times larger than the distance between the tip and the pivot), a typical resolution of 0.1 μm can be easily obtained in measuring the tip displacement. A *Y-Z-θ* stage was designed to mount the PSD and is used in the alignment of the sensor.

The sample is mounted on an *X-Y-Z* micro-stage and its alignment with respect to the tip is monitored by a long working distance optical microscope equipped with a CCD camera connected to a computer with digital frame grabbing hardware (EPIX Inc., PIXCI SV4) and software (EPIX Inc., XCLIBV2.2-DWT-U and XCAPLITE-WIN-V2.2). A wide variety of tip shapes and dimensions are commercially available, which can provide a variety of loading conditions, including point load and line load conditions.

Note that all the controlling and monitoring components, i.e., the upper magnet, the laser, the PSD, and the microscope, are isolated from the rigid beam. This fact significantly reduces the vibration and noise and protects the very fragile structures that are being tested.

The magnetostatic force is actually determined by the difference $\Delta d = d_0 - d$, where d_0 is the initial distance between the magnets at the point where the tip first comes into contact with the sample and d is the distance between the magnets at some arbitrary moment during the experiment (see illustration in Fig. 2). The working conditions are chosen in which $d_0 = 100$ mm and Δd varies up to 13 mm. Under these conditions the sample (or load cell) displacements at the μm scale are negligible in comparison to Δd, and hence $\Delta d \cong \Delta z$, where $\Delta z = z_0 - z$ relates to the absolute readings of the upper magnet position (see Fig. 2). Thus, the load is determined directly by the upper magnet position and load-control conditions are achieved. Moreover, since $d_0 \gg \Delta z$, there is nearly a linear relation between F and Δz, as is demonstrated by the calibration curve presented in Fig. 3, which was measured by placing a load cell (Omega Engineering Inc., LCFA-50g) instead of the sample. It can be deduced from the curve in Fig. 3, a 1 μm change of Δz results in load change of 1.5 μN. Thus, load sensitivity in the μN scale can be easily obtained by moving the upper magnet with a micro-positioning device. Note that different cali-

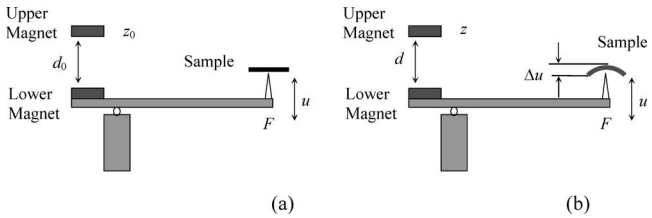

Fig. 2 Schematics of the loading system, (*a*) at the point where the tip first comes into contact with the sample; (*b*) at some arbitrary moment during the experiment. d_0 is the initial distance between the upper and lower magnets at the moment as shown in (*a*); *d* is the distance between the magnets at some arbitrary loading; z_0 is the initial reading of the upper magnets position; *z* is the absolute position at some arbitrary loading moment.

bration curves, which provide different load range and different sensitivity, can be obtained by choosing different values for d_0 or by placing different magnets.

In principle, the sample should be placed at the same height as the load cell in order to obtain the same d_0 value. Nevertheless, changes of d_0 in the range of ±1 mm result only in subtle changes of the calibration curve and hence small changes of the sample height will not have a significant effect on the calibration curve. On the other hand, an accurate determination of z_0, i.e., a clear identification of the point where the tip first comes into contact with the sample, is essential in order to accurately determines Δz. Figure 4 demonstrates that z_0 can be determined with an accuracy which is equivalent to the resolution of the micro-positioning device that is used to move the upper magnet. In this figure, two distinct regions are clearly observed in the plot of the tip displacement, u, as a function of z. During the initial movement of the magnet, the tip does not touch the sample and hence its displacement is proportional to the displacement of the upper magnet and the slope is relatively large. At the point where the tip contacts the sample, the slope changes abruptly, as the tip displacement is now equal to the sample displacement and is in the μm-scale. The obvious change in slope makes it very easy to identify the contact point. The resolution of determining the contact point has the same resolution of the z measurement, i.e., the resolution is on the order of 0.1 μm. As a result, the error in contact force is on the order of sub-μN.

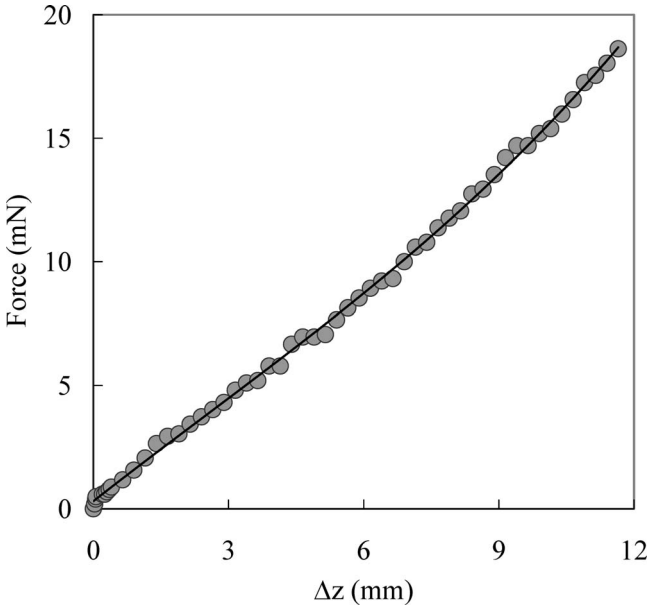

Fig. 3 The applied force, *F* in mN, as a function of the change in the position (displacement) of the upper magnet, Δz in mm for the identical z_0 as in the experiments. This response curve was obtained by applying force on a load cell.

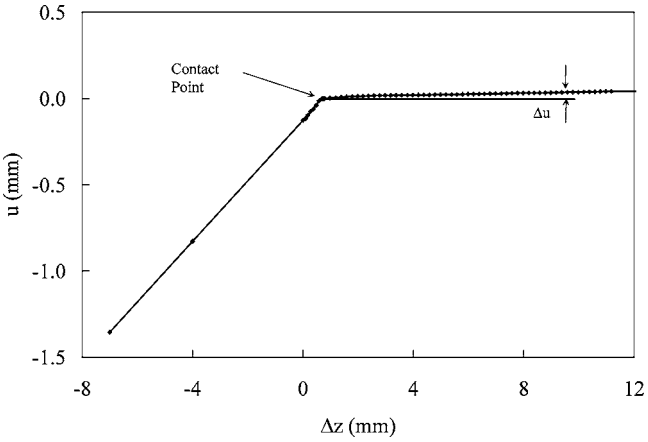

Fig. 4 The tip displacement, *u*, as a function of the position of the upper magnet, *z*. The slope of the curve changes abruptly at the point where the tip first comes into contact with the sample. The maximum value of Δu is less than 50 μm, for a change in position of the upper magnet which is on the order of 10 mm, 3 orders of magnitude larger than Δu. As a consequence, the load is completely determined by *z* and the setup is working in load-control mode.

3 Results

The results presented in this paper were obtained using a ruby ball tip, having a radius, $R=150$ μm. Large tip radius is desired in testing square and rectangular membranes in order to limit the indentation stress and prevent membrane rupture. As shown below, although the tip radius is a significant fraction of the membrane span, the radius of the contact region, r_c, is much smaller than the span, a. This fact significantly simplifies the mechanical analysis.

Figure 5 shows the applied force as a function of the measured tip displacement during loading and unloading processes. The two curves coincide with each other with no significant hysteresis, which means that the membrane behaves elastically. The largest

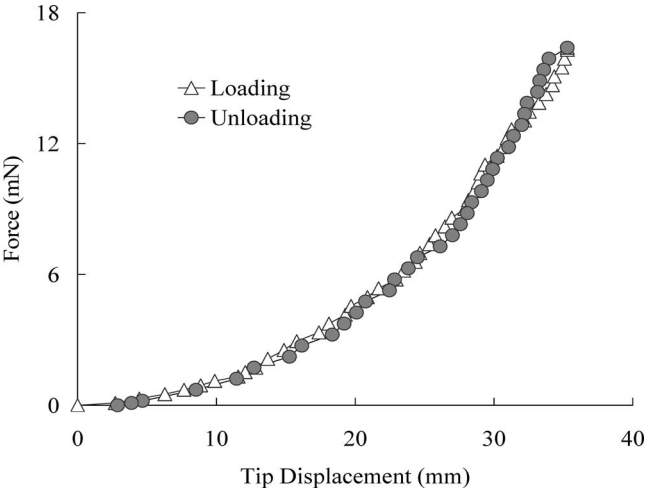

Fig. 5 The mechanical response of a 75 nm thick free-standing amorphous silicon nitride (Si_3N_4) film during loading and unloading

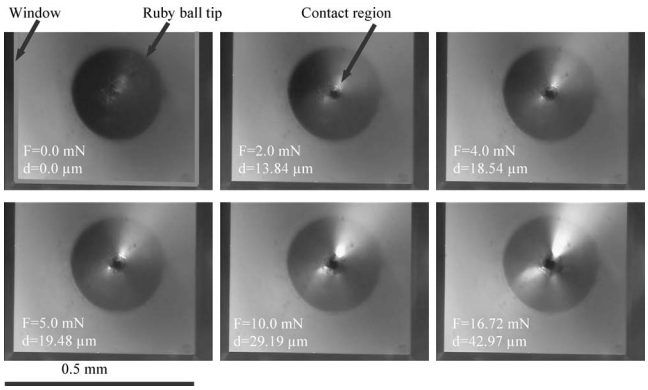

Fig. 6 A series of optical images of a Si_3N_4 membrane under different loads (corresponding load (*F*) and displacement (*d*) are indicated). These images were captured by a CCD camera mounted on the microscope above the membrane. In each image, the gray square is the Si_3N_4 membrane (window); the circular region is the ruby ball tip; the small dark region in the center which expands when loading increases is the contact area.

tip displacement is 37.5 μm, which is about 500 times the film thickness, t. This means that the bending stresses are negligible in comparison to the stresses due to stretching, i.e., to a very good approximation the thin film behaves as a membrane. Figure 6 shows a series of optical images of the membrane, which were taken under different loads. The deflected membrane forms a tent-shape where the angle of deflection, β, increases as the load increases. The repeatability of the new technique is demonstrated in Fig. 7, which presents the load-displacement curves of five membranes located in different regions of the same wafer (see Fig. 7, insert). All the curves are almost coincident with each other.

A geometrical calculation under the assumption of membrane theory shows that the radius of the contact region is given by $r_c = R \sin\beta$ (see Fig. 8). Therefore, for reasonable values of $\beta(0-15$ deg), $r_c \ll R$ and hence $r_c \ll a$, where a is again, the span of the film. Under these conditions the deflection angle can be computed, $\tan\beta = 2u/a$. Thus, for the largest tip displacement of $u = 37.5$ μm, β and r_c take values of 10.2 deg and 26 μm, respectively.

For the membrane theory approximation, the stresses at the

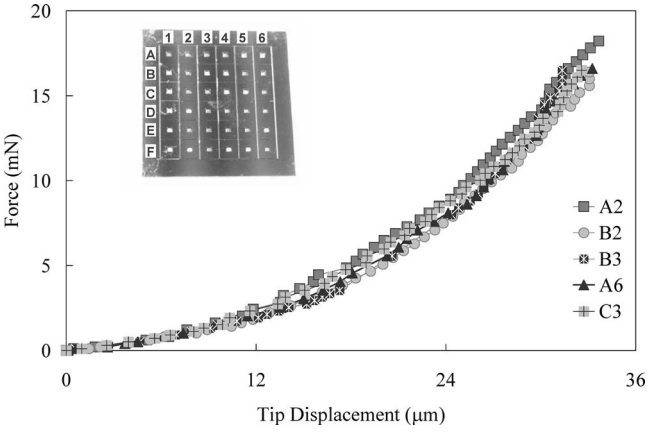

Fig. 7 A wafer consisting of 6×6 devices (insert) was tested at various locations. The mechanical responses of five membranes located at different regions of the same wafer are highly repeatable.

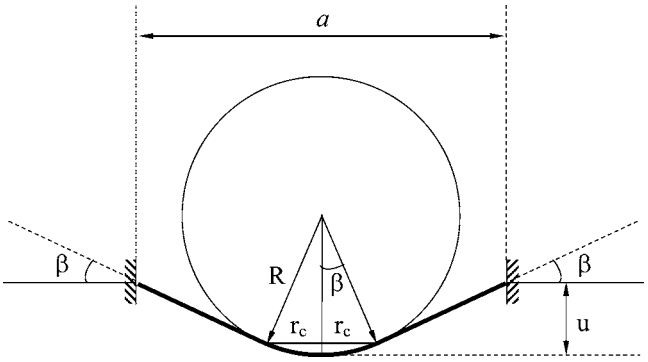

Fig. 8 Schematic diagram of a ridged spherical loading tip deforming a free-standing membrane. The relevant geometric variables are labeled.

contact region are uniform and the balance of the total forces along the z-direction yields the following expression for the membrane (stretching) stress,

$$\sigma = \frac{F}{2\pi t r_c \sin\beta} \cong \frac{Fa^2}{8\pi t R u^2} \tag{1}$$

where t is the membrane thickness, i.e., 75 nm, that of the thin film. The expression on the right hand side in (1) was obtained by making the small angle approximation, i.e., $\sin\beta \cong 2u/a$. A substitution of the largest tip displacement, $u = 37.5$ μm, at the highest force, $F = 16.6$ mN, results in very large membrane stress, $\sigma = 9.2$ GPa.

The attainment of such high stresses and large deflections reflect the high quality of the Si_3N_4 membranes. This also attests to the capabilities of the developed technique to avoid local or transient stress concentrations during the entire approach, loading, and unloading phases of the experiment. It illustrates the capability of the new technique for studying highly fragile and micro devices and structures.

4 Data Analysis and Results

4.1 Finite Element Analysis. The complexity of modeling the mechanical problem associated with the technique developed here is due to the contact loading process and large deformation associated with this problem. As a result, the loading boundary evolves with unknown loading distribution, and the governing equations are strongly coupled with severe nonlinearity even for a simple structure such as a membrane, for which the effect of bending is neglected [20]. Begley [21] recently investigated the axially symmetric case of contact problem and obtained a closed form solution while considering the effect of the indenter size. For the two-dimensional (2D) membrane under pressure loading, the solution to the resulting strongly coupled second-order partial differential equations were obtained numerically [20]. Yet, finding analytical solutions for the combination of these two cases remains as an open problem. In the present investigation, the finite element method is used to simulate tthe mechanical problem of the experiment, namely a spherical indenter loading a thin membrane. The complete analysis consists of two steps. The first step, i.e., the forward analysis, is to simulate an F (force)-d (displacement) curve by assigning a set of known material properties. Following this analysis, the shape factors which describe the response (F-d) curve are obtained by curve fitting and dimensional analysis. During the second step, the reverse analysis, material properties of the membrane are obtained by best fitting the experimental curve.

The simulations were performed using a commercial code, ABAQUS Standard Version 6.4.1 [22]. The geometry of the model has two parts: The indenter and the film. The indenter is simulated

by a rigid sphere with 300 μm in diameter and the free standing film has square geometry of the 470×470 μm with the thickness of 0.1 μm.

The thin film is discretized using 6 or 8 noded 3D continuum elements (C3D6 and C3D8), which can model large deformation problems and provide high accuracy in problems involving contact. There are 14,007 nodes and 7338 elements in the thin film and the region over which the mesh is refined covers the center area of the thin film with 100 μm in diameter. Within this region, the largest element is about 2.5×2.5 μm, and the smallest element size is 0.3×0.3 μm.

The thin film was clamped on all four sides to simulate the boundary condition of being bonded to a rigid substrate. The indenter was confined such that only translation in the z direction (normal to the thin film) was allowed. No additional symmetry conditions were imposed because a complete thin film and indenter geometry was used instead of part of it.

The loading is applied by specifying the axial displacement of the indenter. In the contact pair, the top surface of the film is defined as the slave surface and the spherical surface of the indenter as the master surface. The contact between the thin film and the spherical indenter is assumed to be governed by Coulomb friction law. Because both the materials are ceramics, which tend to have large adhesion, the high stress inside the film indicate that the contact pair could have very strong interaction. For these reasons, rough surface interaction is assumed and the friction coefficient for the contact was set to be 0.8. The effect of the friction coefficient on the results will be discussed later.

The initial material properties for the thin film amorphous Si_3N_4 are chosen to approximate the properties close to that of the bulk ceramic Si_3N_4. Accordingly, the elastic modulus and the Poisson's ratio are chosen to be 300 GPa and 0.22, respectively [23]. The linear elastic material model (elastic constitutive model of ABAQUS) with large deformation capability is chosen based on the experimental observation where there is no hysteresis in the loading-unloading process as indicated by the load-displacement curves (Fig. 5) and the film appeared intact without any cracks after loading when examined using a scanning electron microscope (SEM). The equi-biaxial residual stresses of free-standing thin films are significant parameters which depend largely on the sample fabrication method. The samples used in current investigation were fabricated by the low pressure chemical vapor deposition (LPCVD) Si_3N_4 on Si substrate and then etched away part of the substrate to make the film free-standing. In the analysis, the residual stresses are specified to be 370 MPa in the simulations corresponding to the nominal value often found in the literature for this type of thin film [23].

The indentation displacement is increased monotonically to a maximum displacement of 50 μm in 200 steps. This maximum displacement is larger than the measured experimental displacement. The geometrically nonlinear solver for large deformation in ABAQUS is employed for solving the boundary value problem. At the end of each step, the stress component in the z-direction (vertical) of the indenter is integrated in the contact area to obtain the total indentation force. Thus, the F-d curve is obtained.

4.2 Mechanical Properties Analysis. The first step in extracting the mechanical properties is to obtain the shape factors describing the load-displacement response by curve fitting of the FEA result. The F-d curve is shown in Fig. 9 for the geometrical and material parameters specified in the previous section. It is critical to choose the right form of the relation between the indentation force (F) and the center displacement (d). The solution to corresponding one-dimensional problem [21,24] suggests that two terms should be included in the F-d relation: A linear term and a cubic term with respect to d. The linear term dominates the small deflection regime and is strongly affected by the residual stress. The cubic term that dominates the large deflection regime is strongly influenced by the modulus of the material. The research

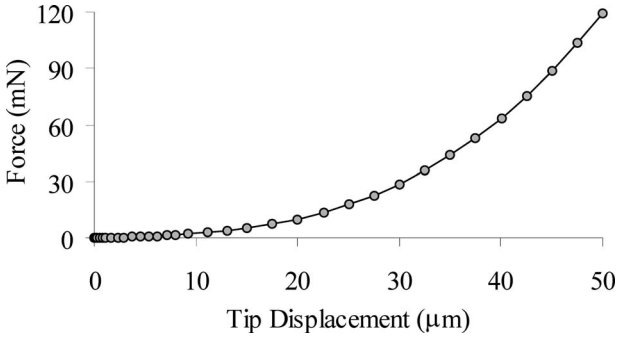

Fig. 9 Load-deflection (F-d) curve obtained from the finite element simulation and is used to obtain the shape factors in Eq. (2). The solid curve is the fit and the solid dots are the finite element analysis data.

on a square membrane under similar contact conditions still remains an open problem. However, it is reasonable to assume that the solution to the square membrane is similar to the circular membrane, except for coefficients (shape factors) to describe the difference in the response (F-d) curves.

Based on the arguments outlined above, the F-d relation is assumed to have the following form,

$$F = C_1 at\left[\sigma_0\left(\frac{d}{a}\right) + C_2\frac{Et^3}{(1-\nu^2)a^3}\left(\frac{d}{a}\right)^3\right] \tag{2}$$

where C_1 and C_2 are dimensionless coefficients.

Equation (2) can be rewritten in the following form,

$$F = A_1 d + A_3 d^3 \tag{3}$$

where A_1 and A_3 are coefficients corresponding to the linear term and cubic term, respectively. The least squares fitting of the F-d curve in Fig. 9 results in the coefficients, $A_1=0.134$ mN/μm and $A_3=9.047\times10^{-4}$ mN/μm^3. Then, for the assumed material properties in the finite element simulations, $E=300$ GPa, $\nu=0.22$ and $\sigma_0=370$ MPa, the shape factors C_1 and C_2 are evaluated to be 3.62 and 1.82×10^{11}, respectively. These shape factors will be used to determine Young's modulus and residual stress in the next step, i.e., the inverse analysis.

Figure 10 shows the least square fitting of the experimental F-d curve. By fitting this curve using Eq. (3), the fitting coefficients, A_1^e and A_3^e, are found to be 0.123 mN/μm and 2.33×10^{-4} mN/μm^3, respectively. The superscript e in the fitting coefficients is used to denote that they correspond to the experi-

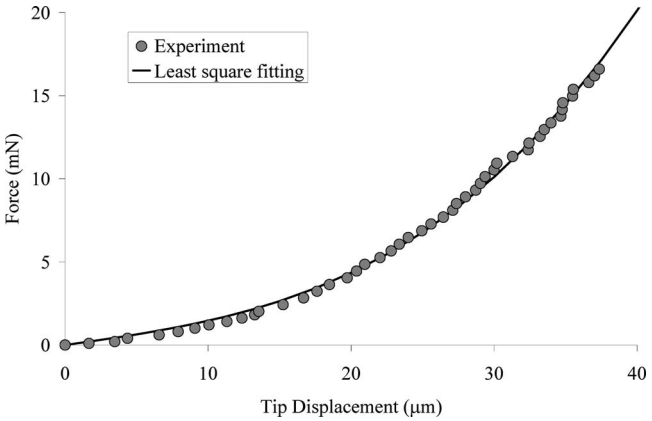

Fig. 10 Least square fitting of force-displacement (F-d) curve of the experimental data for extracting material properties using Eqs. (4) and (5)

Table 1 Comparison of properties for silicon nitride film

Reference	Test Method	Young's Modulus E (GPa)	Residual Stress σ_0 (MPa)	Difference in E (%)
Current work	Contact loading	243	417	0
Edwards et al. [23]	Micro tension	255±5	NA	4.7
Zhang et al. [25]	Pressure buldge	255.3	372	4.7

mentally determined values. Then, the initial stress σ_0 and the elastic modulus E of the film can be obtained as $\sigma_0=417.3$ MPa and $E=243.2$ GPa, by using the following equations:

$$\sigma_0 = \frac{A_1^e}{C_1 t} \tag{4}$$

$$E = \frac{A_3^e(1-\nu^2)a^5}{C_1 C_2 t^4} \tag{5}$$

where C_1 and C_2 are obtained in the first step of the analysis, and equal 3.62 and 1.82×10^{11}, respectively. The values of Young's modulus and residual stress agree well with the characterization results of the same sample by a different technique, the pressure bulge test [25]. The value of the Young's modulus of thin film Si_3N_4 found here is found to be in good agreement with those found in literature [23] (see Table 1).

4.3 Uncertainty Analysis. For a given F-d curve, the solution of E and σ_0 are unique, i.e., there are unique values of fitted E and σ_0. The accuracy of the above analysis directly depends on the accurate measurement of the F-d curve. The errors in the tests come from the displacement and the force measurements. Typical error from displacement measurements is about 0.1 μm over the displacement range of 30 μm, which is less than 0.5%. Errors in the force measurements include a 5% error from the load cell and a less-than 0.1% error from the micrometer. Therefore, the total error in the analysis is about 5.6%.

During the first step of the analysis where the two shape factors C_1 and C_2 are determined, the sensitivity of C_1 and C_2 to the variation of input material properties was investigated. The results showed that a ±5% change in either the Poisson's ratio (ν) or the residual stress (σ_0) would lead to variations of less than ±5% of the shape factors values. When ν reaches 0.25, the maximum value in the reasonable range for Si_3N_4 [23], i.e., a 13% increase value, the result only shows a 3% change in C_1 and C_2. However, these two shape factors are more sensitive to variation in the Young's modulus, E. A 5% change in E will lead a 9% change in C_2 and less than 7% change in C_1. The effect of friction coefficient is also analyzed. To change its value from 0.8 to 1.0 will only lead a 3% change in both C_1 and C_2. Moreover, for a frictionless condition, where this coefficient is zero, it will result in less than 7% change in C_1 and 9% change in C_2.

During the second step of the analysis of determining the material properties, the sensitivity of the predicted material properties to variations in the shape factors obtained from the first step analysis is studied as well. The results showed that a ±5% change of C_1 will cause $\mp$5% change in values of E and σ_0, while a ±5% change in C_2 will introduce $\mp$5% change in E and leave σ_0 unchanged.

In order to verify the method used in current work to obtain material properties, the predicted material properties were used as input in FEM analysis. The calculated F-d curve agrees well with the experimental data. Both the first and second step of the analysis gave unique results of parameters, (C_1, C_2), and (E, σ_0), respectively.

Moreover, the effect of the residual stress on the mechanical behavior of the overall structure cannot be ignored. From (2), one can see that the pre-stress makes the film stiffer, i.e., for the loading with the same magnitude, the pre-stressed (tensile) film will have less center deflection. This feature can be used in MEMS devices to improve the performance. The pre-stress can be as much as several hundred MPa, and this can cause a difference in the center deflection as much as 20%, which could affect the performance of the MEMS devices significantly.

5 Conclusions

A new technique for the mechanical characterization of released thin films under indentation load has been developed. This technique can be used to apply load in the μN-mN range by either load or displacement control. The load and displacement can be measured to an accuracy of within 0.1 mN and 0.1 μm, respectively. The capability and reliability of this new technique has been demonstrated by studying Si_3N_4 free-standing membranes. The elastic modulus and residual stress of Si_3N_4 free standing thin film are around 250 GPa and 400 MPa, respectively. These values are in close agreement with values obtained using a different technique and as well as those found in the literature. The experimental setup has the capability of testing bridge shape samples by using wedge-shaped loading tips instead of spherical (ball) tips. It also has the capability for performing dynamic measurements by replacing the permanent magnets in the current loading apparatus with computer controlled electro-magnets.

Acknowledgment

The research support provided by the Army Research Office through a MURI grant (No. DAAD19-01-1-0517) to the California Institute of Technology on *Engineered Complexity in Ferroelectric Devices* is gratefully acknowledged.

References

[1] Spearing, S. M., 2000, "Materials Issues in Microelectromechanical Systems (MEMS)," Acta Mater., **48**, pp. 179–196.
[2] Sharpe, W. N., 2001, Mechanical Properties of MEMS Materials, in *The MEMS Handbook*, M. Gad-el-Hak, ed., CRC Press, Boca Raton, FL.
[3] Senturia, S. D., 2001, *Microsystem design*, Kluwer Publishers, Boston.
[4] Oliver, W. C., and Pharr, G. M., 1992, "An Improved Technique for Determining Hardness and Elastic Modulus Using Load and Displacement Sensing Indentation Experiments," J. Mater. Res., **7**(6), pp. 1564–1583.
[5] Srikar, V. T., and Spearing, S. M., 2003, "A Critical Review of Microscale Mechanical Testing Methods Used in the Design of Microelectromechanical Systems," Exp. Mech., **43**, pp. 238–247.
[6] Haque, M. A., and Saif, M. T. A., 2003, "A Review of MEMS-Based Microscale and Nanoscale Tensile and Bending Testing," Exp. Mech., **43**(3), pp. 248–255.
[7] Kraft, O., and Volkert, C. A., 2001, "Mechanical Testing of Thin Films and Small Structures," Adv. Eng. Mater., **3**, pp. 99–110.
[8] Zhang, T. Y., Su, Y. J., Qian, C. F., Zhao, M. H., and Chen, L. Q., 2000, "Microbridge Testing of Silicon Nitride Thin Films Deposited on Silicon Wafer," Acta Mater., **48**, pp. 2843–2857.
[9] Vlassak, J. J., and Nix, W. D., 1992, "A New Bulge Test Technique for the Determination of Young's Modulus and Poisson's Ratio of Thin Films," J. Mater. Res., **7**(12), pp. 3242–3249.
[10] Read, D. T., and Dally, J. W., 1993, "A New Method for Measuring the Strength and Ductility of Thin Films," J. Mater. Res., **8**(7), pp. 1542–1549.
[11] Chasiotis, I., and Knauss, W., 2002, "A New Microtensile Tester for the Study of MEMS Materials with the Aid of Atomic Force Microscopy," Exp. Mech., **42**(1), pp. 51–57.
[12] Haque, M. A., and Saif, M. T. A., 2002, "In situ Tensile Testing of Nano-scale Specimens in SEM and TEM," Exp. Mech., **42**, pp. 123–128.
[13] Emery, R. D., and Povirk, G. L., 2003, "Tensile Behavior of Free-standing Gold Films. Part I. Coarse-Grained Films," Acta Mater., **51**, pp. 2067–2078; Acta Mater., **51**, pp. 2079–2087.
[14] Espinosa, H. D., Prorok, B. C., and Fischer, M., 2003, "A Methodology for Determining Mechanical Properties of Freestanding Thin Films and MEMS Materials," J. Mech. Phys. Solids, **51**, pp. 47–67.
[15] Sharpe, W. N., and Gianola, D. S., 2004, "Techniques for Testing Thin Films in Tension," Exp. Tech., **28**, pp. 23–27.
[16] Ruud, J. A., Josell, D., Spaepen, F., and Greer, A. L., 1993, "A New Method for Tensile Testing of Thin Films," J. Mater. Res., **8**(1), pp. 112–117.
[17] Zhu, Y., Moldova, N., and Espinosa, H. D., 2005, "A Microelectromechanical

Load Sensor for In Situ Electron and X-ray Microscopy Tensile Testing on Nanostructures," Appl. Phys. Lett., **86**, 013506.
[18] Shu, Y. C., and Bhattacharya, K., "Domain Patterns and Macroscopic Behavior of Ferroelectric Materials," Philos. Mag. B, **81**(12), (2001).
[19] Burcsu, E., Ravichandran, G., and Bhattacharya, K., "Large Electrostrictive Actuation of Barium Titanate Single Crystals," J. Mech. Phys. Solids, **52**, 823–846 (2004).
[20] Katsikadelis, J. T., Nerantzaki, M. S., and Tsiatas, C. C., 2001, "The Analog Equation Method for Large Deflection Analysis of Membranes. A Boundary-only Solution," Comput. Mech., **27**, pp. 513–523.
[21] Begley, M. R., and Mackin, T. J., 2004, "Spherical Indentation of Freestanding Circular Thin Films in the Membrane Regime," J. Mech. Phys. Solids, **52**, pp. 2005–2023.
[22] ABAQUS, www.abaqus.com
[23] Edwards, R. L., and Sharpe, W. N., 2004, "Comparison of Tensile and Bulge Tests for Thin-film Silicon Nitride," Exp. Mech., **44**, pp. 49–54.
[24] Zhang, Y., and Wise, K. D., 1994, "Performance of Non-Planar Silicon Diaphragms Under Large Deflections," J. Microelectromech. Syst., **3**(2), pp. 59–68.
[25] Zhang, R., Shilo, D., De Basombes, J. T., Bhattcharya, K., and Ravichandran, G., 2005, "Mechanical Characterization of Multi-Layer Free Standing Thin Films Using Pressure Bulge Test," Exp. Mech., in preparation.